Ionics (2018) 24:3431–3437
https://doi.org/10.1007/s11581-018-2528-0

ORIGINAL PAPER

Flower-like MoS_2 supported on three-dimensional graphene aerogels as high-performance anode materials for sodium-ion batteries

Yu Wang[1] · Yuhong Jin[2] · Shubo Li[1] · Jiying Han[1] · Zhendong Ju[1] · Mengqiu Jia[1]

Received: 5 January 2018 / Revised: 4 March 2018 / Accepted: 9 March 2018 / Published online: 26 March 2018

Abstract

Flower-like MoS_2 supported on three-dimensional graphene aerogel (MoS_2/GA) composite has been prepared by a facile hydrothermal method followed by subsequent heat-treatment process. Each of MoS_2 microflowers is surrounded by the three-dimensional graphene nanosheets. The MoS_2/GA composite is applied as an anode material of sodium-ion batteries (SIBs) and it exhibits high initial discharge/charge capacities of 562.7 and 460 mAh g^{-1} at a current density of 0.1 A g^{-1} and good cycling performance (348.6 mAh g^{-1} after 30 cycles at 0.1 A g^{-1}). The good Na^+ storage properties of the MoS_2/GA composite could be attributed to the unique structure which flower-like MoS_2 are homogeneously and tightly decorated on the surface of three-dimensional graphene aerogel. Our results demonstrate that as-prepared MoS_2/GA composite has a great potential prospect as anodes for SIBs.

Keywords MoS_2 · Graphene aerogel · Anode materials · Sodium-ion batteries

Introduction

Sodium-ion batteries (SIBs) have been considered as one of the potential battery systems, which have attracted extensive interest as a candidate to replace lithium-ion batteries (LIBs) owing to the abundance of sodium in the earth [1, 2]. Similar to the LIBs, the major research in SIBs is focused on finding suitable anode materials for reversible and rapid Na^+ storage [3–5]. Among many anode materials, MoS_2 have drawn tremendous attention due to its high theoretical capacity (670 mAh g^{-1}) [6] and low cost. However, the poor ionic, electronic conductivity and the volume variation during cycling further hamper the application of MoS_2 as an anode material of SIBs [7]. Amorphous hard carbons prepared from hydrocarbons, polymers, and biomass with large interlayer distance and disordered structure are promising anode materials for SIBs, but they possess low initial coulombic efficiency [8–12]. Also, graphene has always been used to improve the performance of MoS_2 in many studies due to its good electronic conductivity and mechanical resilience [13]. Recently, Kang's group [14] used a one-pot spray pyrolysis process forming the mixed solution of graphene oxide, $(NH_4)_2MoS_4$, and polystyrene to prepare MoS_2-graphene composite which shows superior electrochemical properties. Xiang et al. [15] reported a single-mode microwave-assisted method using 3D graphene foam as a substrate to obtain MoS_2/graphene nanocomposites. The as-prepared MoS_2/graphene nanocomposites showed a high reversible capacity of 290 mAh g^{-1} at 0.1 A g^{-1} after 100 cycles. Wang and coworkers [16] reported that expanded MoS_2/G composite, which was prepared by the attachment of expanded MoS_2 layers onto graphene sheets by a simple hydrothermal method, exhibited electrochemical properties for SIBs. The role of heterointerface between graphene and MoS_2 was in-depth studied by Wang's group [17]. The MoS_2/RGO heterointerface can enhance the electronic conductivity of MoS_2 and store more Na^+; MoS_2/RGO composites retained a stable capacity of 227 mAh g^{-1} at 320 mA g^{-1} for 300 cycles.

However, to the best of our knowledge, there are few reports on the preparation of flower-like MoS_2 grown on 3D graphene for the application of SIBs by a facile hydrothermal

✉ Yuhong Jin
jinyh@bjut.edu.cn

✉ Mengqiu Jia
jiamq@mail.buct.edu.cn

[1] Beijing Key Laboratory of Electrochemical Process and Technology for Materials, Beijing University of Chemical Technology, Beijing 100029, China

[2] Beijing Guyue New Materials Research Institute, Beijing University of Technology, Beijing 100124, China

method. Therefore, we reported the preparation of flower-like MoS_2-graphene aerogel using a facile hydrothermal strategy and subsequently heat-treatment process. Benefitting from the flower-like MoS_2 grown on the conductive network GA, the as-prepared composites produce more active reaction sites of Na^+ storage and enhance the conductivity and stability of the active materials.

Experimental section

Preparation of flower-like MoS_2-graphene aerogel composites

Graphene oxide (GO) was synthesized using a modified Hummers' method [18]. As shown in Fig. 1, 50 mL GO aqueous dispersion (2 mg mL^{-1}) was poured into 100-mL Teflon-lined stainless steel autoclave and reacted at 180 °C for 12 h. The GA was obtained after freeze-dried. 8.3732 g thiourea, 100 mg GA, and 8.8277 g ammonium heptamolybdate were dissolved into 50 mL 1 M NaOH solution; then, the stable suspension was transferred into 100-mL Teflon-lined stainless steel autoclave and heated to 220 °C for 10 h. The sample was washed, freeze-dried, and finally annealed at 450 °C for 5 h with a heating rate of 5 °C min^{-1} under a N_2 atmosphere to obtain MoS_2/GA. Bare MoS_2 was synthesized by similar method without adding GA.

Characterization

The morphologies were obtained by scanning electron microscopy (FESEM, JSM-7001F) and high-resolution transmission electron microscopy (HRTEM, JEOL JEM-3010). The crystalline structure was characterized by X-ray diffraction (XRD) measurements on Rigaku D/max-2500 with Cu Kα radiation (=1.54056 Å). Raman spectra were recorded on a JY HR800 with 532-nm laser excitation. The thermal gravimetric analysis (TGA) was performed in air at heating rate of 10 °C min^{-1} on (TGA/DSC 1/1100 SF). The Brunauer-Emmet-Teller (BET) surface areas of as-synthesized samples were carried out by a Micromeritics Model ASAP 2460.

Electrochemical testing

The working electrodes were prepared by mixing the active materials, conducting agent and binder (sodium alginate) with a ratio of 8:1:1 in *N*-methyl-2-pyrrolidone. The slurries were transferred onto copper foil and dried at 120 °C for 12 h in a vacuum oven. The coin cells were assembled in an argon-filled glove box (Mikrouna, H_2O, $O_2 < 0.1$ ppm). Sodium metal was used as counter electrode, glass fiber as separator, and 1 M $NaClO_4$ with 1:1 (*v*/*v*) mixture of ethylene carbonate (EC) and diethyl carbonate (DEC) as the electrolyte. Cyclic voltammetry (CV, 0.1 mV s^{-1}, 0.01–3 V vs Na^+/Na) and electrochemical impedance spectra (EIS, 100 kHz–0.01 Hz) were carried out on a CS310 electrochemical workstation. The galvanostatic charge-discharge test was performed using Neware battery tester (Shenzheng, China).

Results and discussion

Figure 2a represents the XRD patterns of the MoS_2 and MoS_2/GA composite. Both samples show obvious peaks located at $2\theta = 13.5°$, 32.4°, 35.8°, 43°, and 57° that correspond to the (002), (100), (103), (105), and (110) planes, respectively, which can be ascribed to hexagonal MoS_2 (JCPDS No. 37-1492). Furthermore, the (002) diffraction peak demonstrates the presence of MoS_2 layers [19]. Raman spectra of the GO and MoS_2/GA are showed in Fig. 2b. All of spectra display two prominent peaks at ~ 1350 (D band) and ~ 1590 cm^{-1} (G band), which correspond to structure defect and the vibration of sp^2 bonded carbon atoms, respectively

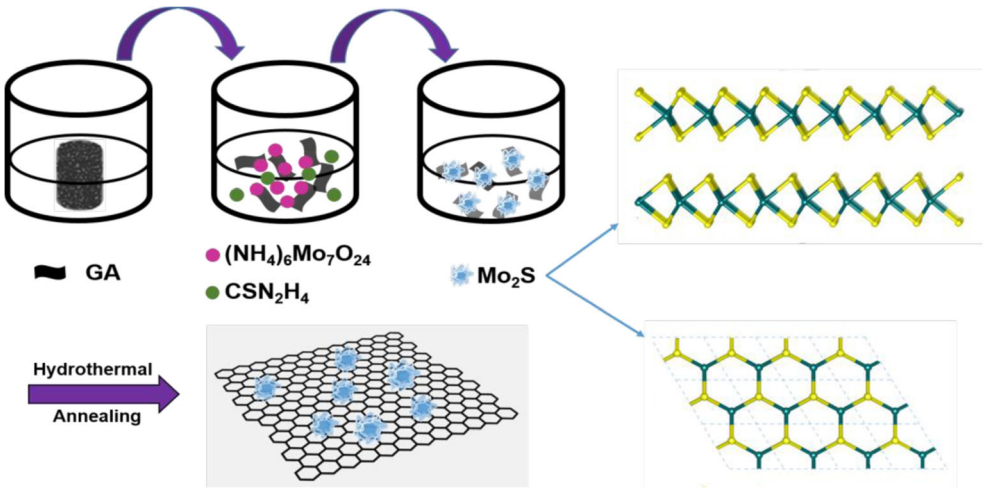

Fig. 1 Scheme of the synthetic process of MoS_2/GA composite

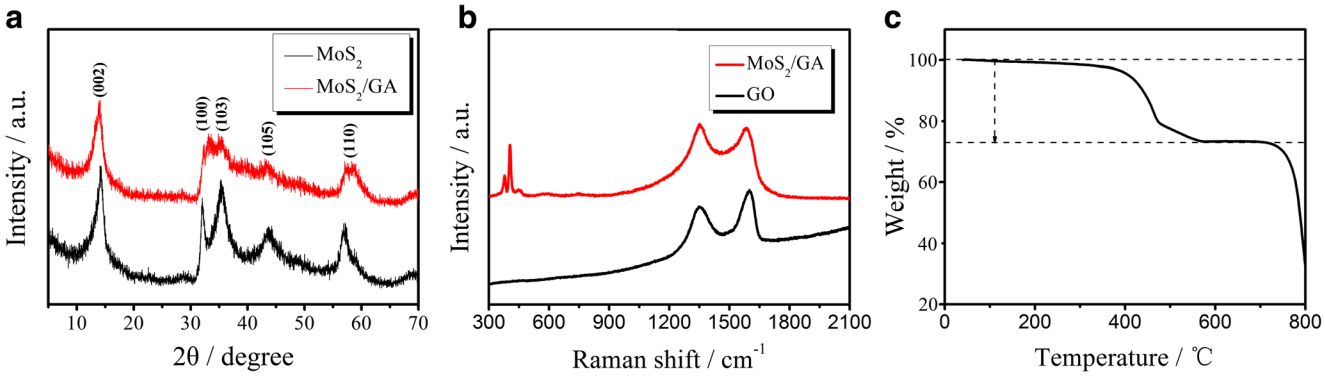

Fig. 2 **a** XRD patterns of MoS_2 and MoS_2/GA composite and **b** Raman spectra of GO and MoS2/GA composite. **c** Thermogravimetric curves of MoS_2/GA composite in air with a heating rate of 10 °C min^{-1}

[20]. The ID/IG value of MoS_2/GA (1.13) is higher than that of GO (0.90), which suggests more defects on GA. In addition, the spectrum of MoS_2/GA exhibits two additional peaks located at 378 and 403 cm^{-1}, respectively, which are assigned to the E^1_{2g} and A_{1g} modes of hexagonal MoS_2. Therein, the E^1_{2g} mode originates from the opposite vibration of two S atoms with regard to the Mo atom, while the A_{1g} mode associated with the out-of-plane vibration of only S atoms along the *c* axis [21]. These results confirm MoS_2 has been combined with GA. Thermogravimetric analysis (TGA) in Fig. 2c was employed to investigate the weight contents of MoS_2 in the composites. The weight decline appears at 400 °C can be ascribed to the oxidation of MoS_2 to MoO_3. The weight loss occurs at approximately 450 °C could be contributed to the oxidation of carbon in air. The sample after 550 °C in the TGA process is pure MoO_3, which has a weight content of 72.8%. The MoS_2 content in the MoS_2/GA is calculated to be 82.1% [22].

X-ray photoelectron spectra (XPS) were performed to investigate the interfacial nature between graphene and MoS_2 as shown in Fig. 3. XPS spectra in Fig. 3a show that MoS_2/GA sample contains Mo, S, C, and O elements. The high-resolution Mo 3d, S 2p, and C 1s XPS spectra of MoS_2/GA are shown in Fig. 3b~d. The C 1s peak is composed of two distinct divided peaks: the C–C at 284.8 eV and C–OH, C–OH at 286.2 eV. On the contrary, carbonyl and carboxylates peaks at 288.4 eV cannot be observed demonstrating the reduction of GO. Mo 3d spectra consists of two peaks located at 229.4 and 232.6 eV confirming the Mo^{4+} in MoS_2. S $2p_{3/2}$ and S $2p_{1/2}$ are located at 162.3 and 163.4 eV, respectively, which are corresponding to the S^{2-} in MoS_2. The high-resolution spectrum of O 1s in Fig. 3e can be resolved into three components, C=O at 531.2 eV, C–OH at 533.3 eV, and a new peak at 532.4 eV [23]. The peak indicates the C–O-metal bond reported before. Therefore, we can conclude that the presence of interfacial interaction between flower-like MoS_2 and graphene is possible proposed by the formation of the C–O–Mo bonds as shown in Fig. 3f [24, 25].

The FESEM and TEM images (as shown in Fig. 4a–e) revealed the morphologies of the MoS_2/GA composite. In Fig. 4a, the flower-like MoS_2 with a high degree of aggregation and large diameter can be observed without the addition of GA. On the contrary, as shown in Fig. 4b–d, flower-like MoS_2 composed of homogeneous nanosheets is deposited on the surface of GA without aggregation. Flower-like MoS_2 has an intimate contact with GA. The clear lattice fringe separated by 0.69 nm observed in the edge part shown by arrows in Fig. 4e corresponds to the (002) plane of the layered MoS_2. This expanded interlayer (0.69 nm) is larger than the reported value (0.67 nm) based on graphene-like MoS_2 nanoflowers [3]. And the selected area electron diffraction (SAED) pattern (as shown in Fig. 4f) shows several clear rings, which are assigned to the (100), (103), and (110) crystal planes of the MoS_2, respectively, demonstrating the crystalline of the MoS_2 [26].

The porous properties of the MoS_2 and MoS_2/GA samples were performed by nitrogen sorption measurements. As plotted in Fig. 5a, MoS_2/GA presents a type IV hysteresis loop (IUPAC classification), which may be closely related to the flower-like particles and GA porous frameworks, in accordance with the morphologies observed in the FESEM images. The BET surface areas of the MoS_2 and MoS_2/GA are 2.6 and 36.7 $m^2\ g^{-1}$, respectively. Obviously, the surface area of MoS_2/GA is much larger than that of the pure MoS_2, attributing to the flower-like nanostructure of MoS_2 and porous network of GA, which can provide a large surface area for double-layer charge storage. The DFT pore size distribution of the MoS_2 and MoS_2/GA samples is shown in Fig. 5b, revealing the presence of hierarchical porosity: from mesopores to macropores. The 3D interconnected porous network consisted of multilevel pores can provide not only plenty transport channels for electrolyte but also strong mechanical strength. Based on the abovementioned reasons, the MoS_2/GA can be employed as an outstanding electrode material for sodium-ion battery [27].

The electrochemical performance of MoS_2/GA composites were further evaluated as an anode material for SIBs.

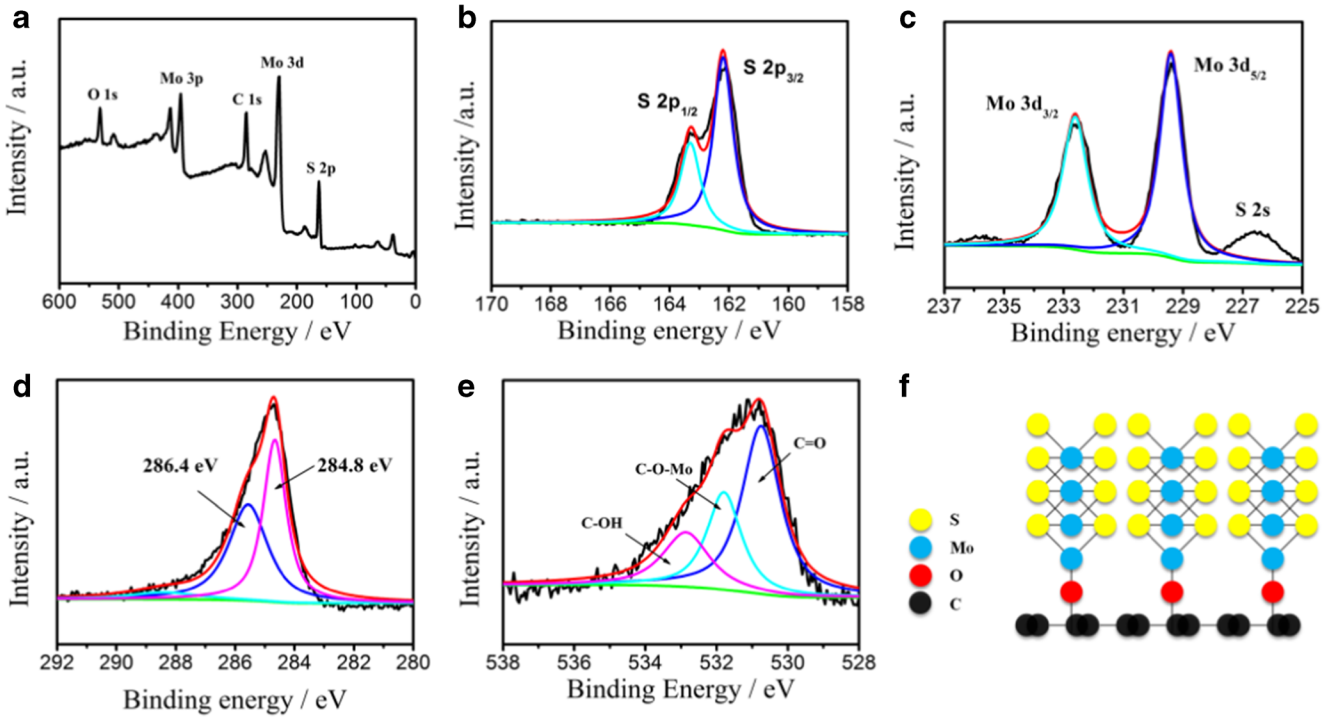

Fig. 3 **a** XPS survey spectrum, high-resolution. **b** S 3p spectrum. **c** Mo 3d spectrum. **d** C 1s spectrum. **e** O 1s spectrum of MoS_2/GA. **f** Illustration of C–O–Mo bond between MoS_2 and GA

Figure 6a displays the CV curves of the MoS_2/GA composites for the first three cycles. In the first cathodic scan, the reduction peaks at 0.8 V is associated with the Na^+ insertion into the MoS_2 and the formation of the solid electrolyte interface (SEI) film. The peak under 0.6 V in the deep cathodic process could be assigned to the electrochemical decomposition of MoS_2 to form metallic Mo embedded in an amorphous Na_2S matrix. In the first anodic process, a broaden oxidation peak was recorded at 1.7 V due to the oxidation of the Mo to MoS_2. The CV peaks in the subsequent cycles are overlapped suggesting high reversibility and cycling stability of Na^+ storage in the MoS_2/GA [28]. The overall reaction can be described by the following equation:

$$MoS_2 + 4Na^+ + 4e^- \leftrightarrow Mo + 2Na_2S$$

In Fig. 6b, the first, second, and third charge-discharge curves of MoS_2/GA at 100 mA g^{-1} were evaluated. The potential plateaus of the first discharge and charge curve for our

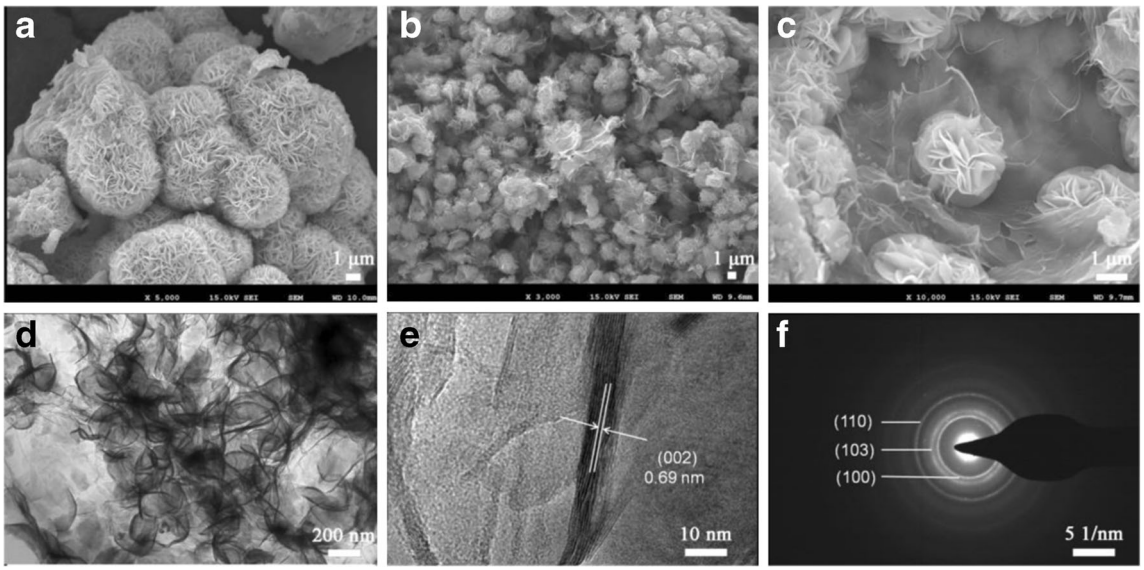

Fig. 4 **a** FESEM image of MoS_2. **b**, **c** FESEM images of MoS_2/GA. **d** TEM image and **e** HRTEM image of MoS_2/GA. **f** SAED pattern of MoS_2/GA

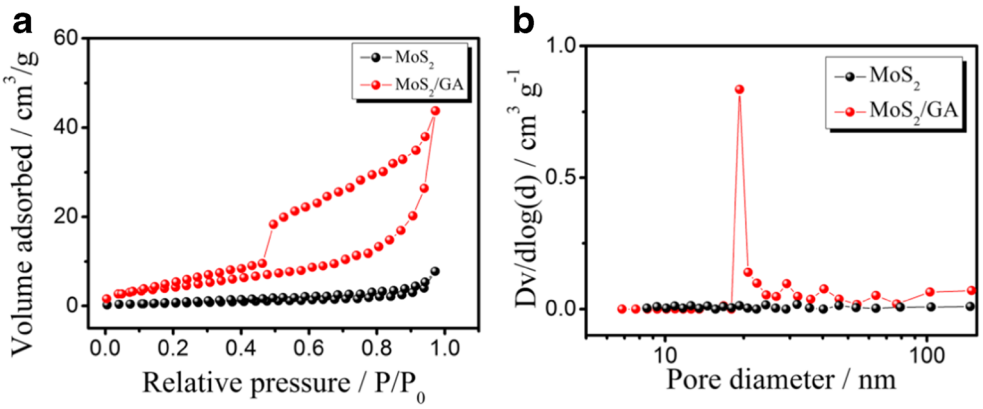

Fig. 5 **a** Nitrogen adsorption/desorption isotherms and **b** the corresponding pore size distribution curves of MoS_2 and MoS_2/GA

MoS_2/GA composite are consistent with the CV results. The initial discharge and charge specific capacities of MoS_2/GA composites are 562.7 and 460 mAh g^{-1}, respectively. The initial coulombic efficiency is 81.7% for the first cycle. High specific capacity over 348.6 mAh g^{-1} can be obtained within 30 cycles at a current density of 100 mA g^{-1} (Fig. 6c). And the specific capacity of MoS_2 and GA are 115 and 107 mAh g^{-1}, respectively. For the rate capability, the discharge capacities were 375, 391, 356, and 208 mAh g^{-1} when cycled at current densities of 50, 100, 250, and 500 mA g^{-1}, respectively (Fig. 6d). And the specific capacity restores to 403 mAh g^{-1} when cycled at 50 mA g^{-1} again [29].

To explore the reason of good electrochemical performance of MoS_2/GA, EIS measurements were calculated after three cycles as shown in Fig. 7. The medium-frequency semicircle is related to the charge transfer resistance (R_{ct}) through the electrode/electrolyte interface. The high-frequency semicircle is related to the solid-state interface layer formed on the surface of the electrodes (R_f). It can be seen that R_{ct} of MoS_2/GA is evident lower than that of MoS_2, suggesting that the composite possess much higher charge transfer efficiency and the consequent rapid electron transport in the Na+ insertion/extraction process due to the introduction of GA [14].

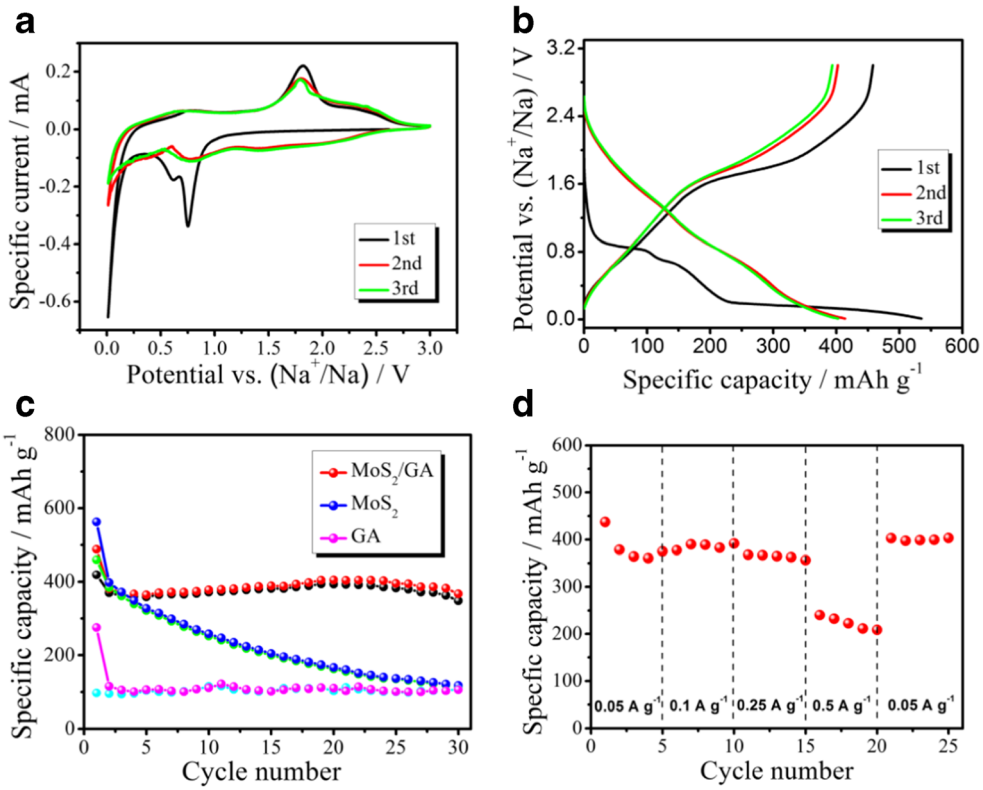

Fig. 6 **a** CV curves of MoS_2/GA measured at 0.1 mV s^{-1}. **b** Charge/discharge curves profiles of MoS_2/GA for the first, second, and third. (c) Cycling performance of GA, MoS_2, and MoS_2/GA. **d** Rate performance of MoS_2/GA

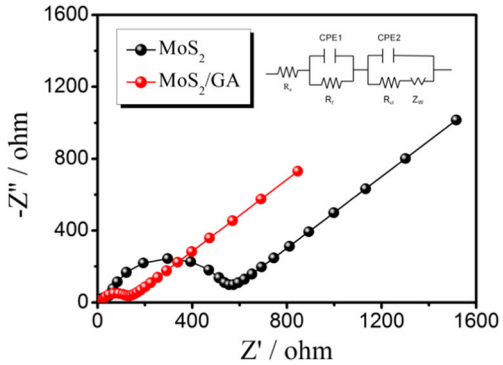

Fig. 7 Nyquist plots of MoS_2/GA and MoS_2. Inset shows the equivalent circuit which can be used to fit the experimental data

Conclusions

In summary, MoS_2/GA composite with superior Na^+ storage was prepared by a facile hydrothermal method. The MoS_2/GA electrodes for sodium storage are benefited from the combination of flower-like MoS_2 and 3D graphene. On the one hand, the flower-like MoS_2 was assembled on the highly conductive 3D graphene, which provides more sodium storage sites for the higher capacity. Moreover, the 3D graphene structure offers sufficient void spaces for volume expansion and fast electron transfer pathways which could buffer the strain during the cycling process. This work provides an effective process on synthesizing 3D metal sulfide-graphene and a potential anode material for SIBs.

References

1. Xiao Y, Lee SH, Sun YK (2016) The application of metal sulfides in sodium ion batteries. Adv Energy Mater:1601329
2. Zhang X, Lai ZC, Tan CL, Zhang H (2016) Solution-processed two-dimensional MoS_2 nanosheets: preparation, hybridization, and applications. Angew Chem Int Ed 55:8816–8838
3. Hu Z, Wang LX, Zhang K, Wang JB, Cheng FY, Tao ZL, Chen J (2014) MoS_2 nanoflowers with expanded interlayers as high-performance anodes for sodium-ion batteries. Angew Chem 126: 13008–13012
4. Ma GY, Huang KS, Zhuang QC, Ju ZC (2016) Superior cycle stability of nitrogen-doped graphene nanosheets for Na-ion batteries. Mater Lett 174:221–225
5. Zhou KQ, Zhen YC, Hong ZS, Guo JH, Huang ZG (2017) Enhanced sodium ion batteries performance by the phase transition from hierarchical Fe_2O_3 to Fe_3O_4 hollow nanostructures. Mater Lett 190:52–55
6. Wang J, Luo C, Gao T, Langrock A, Mignerey A, Wang C (2015) An advanced MoS_2/carbon anode for high-performance sodium-ion batteries. Small 11:473–481
7. Stephenson T, Li Z, Olsenab B, Mitlin D (2014) Lithium ion battery applications of molybdenum disulfide (MoS_2) nanocomposites. Energy Environ Sci 7:209–231
8. Sun N, H Liu BX (2015) Facile synthesis of high performance hard carbon anode materials for sodium ion batteries. J Mater Chem A 3: 20560–20566
9. Xu B, Wang HR, Zhu QZ, Sun N, Anasori B, Hu LF, Wang F, Guan YB, Gogotsi Y (2018) Reduced graphene oxide as a multifunctional conductive binder for supercapacitor electrodes. Energy Storage Mater 12:128–136
10. Liu H, Jia MQ, Cao B, Chen RJ, Lv XY, Tang RJ, Wu F, Xu B (2016) Nitrogen-doped carbon/graphene hybrid anode material for sodium-ion batteries with excellent rate capability. J Power Sources 319:195–201
11. Liu H, Jia MQ, Zhu QZ, Cao B, Chen RJ, Wang Y, Wu F, Xu B (2016) 3D-0D graphene-Fe_3O_4 quantum dot hybrids as high-performance anode materials for sodium-ion batteries. ACS Appl Mater Interfaces 8:26878–26885
12. Liu H, Jia MQ, Yue SF, Cao B, Zhu QZ, Sun N, Xu B (2017) Creative utilization of natural nanocomposites: nitrogen-rich mesoporous carbon for high performance sodium ion battery. J Mater Chem A 5:9572–9579
13. Wang TY, Chen SQ, Pang HP, Xue HG, Yu Y (2017) MoS_2-based nanocomposites for electrochemical energy storage. Adv Sci: 1600289
14. Choi SH, Ko YN, Lee JK, Kang YC (2015) 3D MoS_2-graphene microspheres consisting of multiple nanospheres with superior sodium ion storage properties. Adv Funct Mater 25:1780–1788
15. Xiang JY, Dong DD, Wen FS, Zhao J, Zhang XY, Wang LM, Liu ZY (2016) Microwave synthesized self-standing electrode of MoS_2 nanosheets assembled on graphene foam for high-performance Li-Ion and Na-Ion batteries. J Alloys Comp 660:11–16
16. Wang YX, Chou SL, Wexler D, Liu HK, Dou SX (2014) High-performance sodium-ion batteries and sodium-ion pseudocapacitors based on MoS_2/graphene composites. Chem Eur J 20:9607–9612
17. Xie X, Ao Z, Su D, Zhang J, Wang G (2015) MoS_2/graphene composite anodes with enhanced performance for sodium-ion batteries: the role of the two-dimensional heterointerface. Adv Funct Mater 25:1393–1403
18. Hummers WS, Offeman RE (1958) The preparation of graphite oxide. J Am Chem Soc 80:1339
19. Sun TH, Li ZP, Liu XH, Ma LM, Wang JQ, Yang SG (2016) Facile construction of 3D graphene/MoS_2 composites as advanced electrode materials for supercapacitors. J Power Sources 331:180–188
20. Liu H, Jia M, Sun N, Cao B, Chen R, Zhu Q, Wu F, Qiao N, Xu B (2015) Nitrogen-rich mesoporous carbon as anode material for high-performance sodium-ion batteries. ACS Appl Mater Interfaces 7:27124–27130
21. Qin W, Chen TQ, Pan LK, Niu LY, Hu BW, Li DS, Li JL, Sun Z (2015) MoS_2-reduced graphene oxide composites via microwave assisted synthesis for sodium ion battery anode with improved capacity and cycling performance. Electrochim Acta 153:55–61
22. Pan FS, Wang JQ, Yang ZZ, Gu L, Yu Y (2015) MoS_2-graphene nanosheet-CNT hybrids with excellent electrochemical performances for lithium-ion batteries. RSC Adv 5:77518–77526
23. He JR, Lia PJ, Lv WQ, Wen KC, Chen YF, Zhang WL, Lia YR, Qin W, He WD (2016) Three-dimensional hierarchically structured aerogels constructed with layered MoS_2/graphene nanosheets as free-standing anodes for high-performance lithium ion batteries. Electrochim Acta 215:12–18
24. Long H, Trochimczyk AH, Pham T, Tang ZR, Shi TL, Zettl A, Carraro C, Worsley MA, Maboudian R (2016) High surface area MoS_2/graphene hybrid aerogel for ultrasensitive NO_2 detection. Adv Funct Mater 26:5158–5165
25. Zhou GM, Wang DW, Yin LC, Li N, Li F, Cheng HM (2012) Oxygen bridges between NiO nanosheets and graphene for improvement of lithium storage. ACS Nano 6:3214–3223
26. Zhao B, Wang ZX, Gao Y, Chen L, Lu MN, Jiao Z, Jiang Y, Ding YZ, Cheng LL (2016) Hydrothermal synthesis of layer-controlled MoS_2/graphene composite aerogels for lithium-ion battery anode materials. Appl Surf Sci 390:209–215

27. Qin W, Chen TQ, Pan LK, Niu LY, Hu BW, Li DS, Li JL, Sun Z (2015) MoS_2-reduced graphene oxide composites via microwave assisted synthesis for sodium ion battery anode with improved capacity and cycling performance. Electrochim Acta 153:55–61
28. Sahu TS, Mitra S (2015) Exfoliated MoS_2 sheets and reduced graphene oxide an excellent and fast anode for sodium-ion battery. Sci Rep 5:12571
29. Xiong FY, Cai ZY, Qu LB, Zhang PF, Yuan ZF, Asare OK, Xu WW, Lin C, Mai LQ (2015) Three-dimensional crumpled reduced graphene oxide/MoS_2 nanoflowers: a stable anode for lithium-ion batteries. ACS Appl Mater Interfaces 7:12625–12630